Interlaminar and intralaminar fracture resistance of recycled carbon fibre/PPS composites with tailored fibre/matrix adhesion

Quan, Dong; Liu, Jiaming; Yao, Liaojun; Dransfeld, Clemens; Alderliesten, René; Zhao, Guoqun

DOI
10.1016/j.compscitech.2023.110051

Publication date
2023

Document Version
Final published version

Published in
Composites Science and Technology

Citation (APA)
Quan, D., Liu, J., Yao, L., Dransfeld, C., Alderliesten, R., & Zhao, G. (2023). Interlaminar and intralaminar fracture resistance of recycled carbon fibre/PPS composites with tailored fibre/matrix adhesion. *Composites Science and Technology*, *239*, Article 110051. https://doi.org/10.1016/j.compscitech.2023.110051

Composites Science and Technology 239 (2023) 110051

Contents lists available at ScienceDirect

Composites Science and Technology

journal homepage: www.elsevier.com/locate/compscitech

Interlaminar and intralaminar fracture resistance of recycled carbon fibre/PPS composites with tailored fibre/matrix adhesion

Dong Quan [a,b], Jiaming Liu [a], Liaojun Yao [c], Clemens Dransfeld [b], René Alderliesten [b,*], Guoqun Zhao [a,*]

[a] Key Laboratory for Liquid-Solid Structural Evolution and Processing of Materials (Ministry of Education), Shandong University, PR China
[b] Department of Aerospace Structures and Materials, Delft University of Technology, The Netherlands
[c] Department of Astronautics Science and Mechanics, Harbin Institute of Technology, PR China

ARTICLE INFO

Keywords:
A: Polymer-matrix composites (PMCs)
B: Recycling
B Fibre/matrix bond
B: Fracture toughness
D: Fractography

ABSTRACT

The production of advanced composites from recycled carbon fibres (rCFs) is critical for the sustainable development of carbon fibre industry. Herein, non-woven mats consisting of commingled rCFs and Polyphenylene-sulfide (PPS) fibres were compression moulded to manufacture rCF/PPS composites, with the fibre/matrix adhesion being tailored by UV-irradiating the non-woven mats. The intralaminar and interlaminar fracture resistance and mechanical performance of the rCF/PPS composites were characterised. The experimental results had demonstrated that improving the PPS/rCF adhesion of the composites significantly increased the intralaminar fracture energies and mechanical properties under tensile and shear loading conditions. However, it also negatively affected the interlaminar fracture resistance. The main fracture mechanism was observed to be fibre evulsion for the intralaminar fracture mode, while crack bridging by the rCFs was the primary fracture mechanism for the interlaminar fracture condition. That led to the contrary influences of the improved fibre/matrix adhesion on the intralaminar and interlaminar fracture resistance of the rCF/PPS composites. In summary, this study had shedded lights on tailoring the crack resistance and mechanical performance of rCFRPs by adjusting the fibre/matrix adhesion using the UV-treatment technique.

1. Introduction

The global demanding of strong and light-weight carbon fibre composites has considerably increased in recent years. Accordingly, the amount of carbon fibre composite wastes, including end-of-life products, out-of-date prepregs, trimmed-off materials and experimentally tested specimens has already reached a high level, with a more rapid growth being expected in a short future. This raised significant concerns about environmental pollution, and led to the introduction of strict governmental legislation in many countries regarding the waste management [1–3]. For this reason, extensive attention has been paid to the recovering and recycling of carbon fibres from composite waste.

Currently, the most studied technologies for carbon fibre recycling include solvolysis, pyrolysis and a fluidised bed process [2,4–6]. Among these technologies, pyrolysis is entering a mature stage, e.g. ELG Ltd. has commercialised a number of recycled carbon fibre (rCF) products based on aerospace-grade laminate waste. Recycled carbon fibres are typically in a discontinuous and random form due to the cutting process during the composite manufacturing and the size reduction during the recycling process. Encouragingly, the recycled carbon fibres typically possessed more or less the same mechanical properties as the virgin fibres [2,7,8]. Hence, it is key to develop recycled carbon fibre reinforced plastics (rCFRPs) that can effectively utilise the good mechanical properties of the discontinuous and random distributed rCFs.

Different types of methods were proposed for the re-impregnation of rCFs to manufacture rCFRPs, among which, the compression moulding of intermediate non-woven mats proved to obtain rCFRPs with relatively high fibre volume fractions and hence good mechanical properties [9,10]. The most prevalent techniques for producing intermediate non-woven mats include paper-making method, wet dispersion, carding process and 3-DEP process (deposition of rCFs on a 3D forming screen) [7]. Pimenta [11] et al. used a paper-making process to prepare intermediate non-woven mats based on rCFs and then compression moulding them with epoxy resin layers to manufacture rCFRPs. The nominal volume fraction of the rCFRPs was found to be around 30%, which resulted in essentially the same specific stiffness and strength as the aerospace grade 2024-T4 Aluminium alloy. More encouragingly, the rCFRPs exhibited superior specific stiffness and strength to those of the virgin glass fibre composites that were used in aircraft interiors.

* Corresponding authors.
E-mail addresses: R.C.Alderliesten@tudelft.nl (R. Alderliesten), zhaogq@sdu.edu.cn (G. Zhao).

https://doi.org/10.1016/j.compscitech.2023.110051
Received 3 March 2023; Received in revised form 16 April 2023; Accepted 19 April 2023
Available online 24 April 2023

Similarly, Wei [12] et al. used a paper-making process to manufacture intermediate non-woven mats consisting of rCFs and PA6 fibres. A compression moulding process was then applied to the non-woven mats, during which, the PA6 fibres melted and turned into the matrix of the rCF composites. A maximum fibre volume fraction of 23% was obtained. It was observed that a pressure of at least 5 MPa was needed to obtain good impregnation of the rCFs. Nevertheless, damage to the rCFs was observed if the compression pressure was higher than 8 MPa, that led to negative effects to the mechanical properties of the rCFRPs. Apart from compression moulding of randomly orientated rCFs to manufacture rCFRPs, many studies had attempted to align the discontinuous rCFs using different techniques [13–16] prior to the re-impregnation. In general, obvious increases in the fibre volume fractions and mechanical properties of the rCFRPs could be achieved by the high-level of alignment of the discontinuous rCFs. However, these alignment techniques are far from large-scale engineering applications, owing to the low production efficiency and high cost.

Improving the bonding strength at the rCF/matrix interface is another routine to enhance the mechanical properties of rCFRPs. In general, the fibre sizing on the carbon fibres are decomposed simultaneously with the matrix resin during a recycling process. This can cause significant drops in the fibre/matrix interfacial adhesion for the rCFRPs. For example, Jiang and Pickering [17] observed a 24% reduction in the fibre/epoxy interfacial shear strength due to a 2.6–42% decrease in the oxygen concentration of the fibre surface after a pyrolysis recycling process. Accordingly, additional surface treatment to the rCFs is required to achieve sufficient fibre/matrix adhesion prior to the re-impregnation. A number of methods have been developed to treat the surfaces of the carbon fibres, including electrochemical treatment [18–20], plasma treatment [21–23], chemical oxidation [24–26] and superheated steam oxidation [27]. Feng et al. [26] cleaned the surfaces of rCFs using concentrated nitric acid, and then modified their surfaces with a DGEBA coupling agent. This surface treatment process proved to significantly enhance the rCF/Nylon 6 matrix adhesion, that resulted in remarkable improvements in the tensile modulus and strength, flexural modulus and strength, impact resistance and thermal stability of the rCFRPs. Li et al. [20] applied an electrochemical oxidation method to treat the surfaces of rCFs, that increased the compressive and flexural strengths of the rCFRPs by 25% and 19%, respectively. While surface treatment was typically applied solely to the rCFs in other literatures, it is also appealing to fictionalise the polymer matrix to further enhance the rCF/matrix adhesion. This is especially important for the majority of the semi-crystalline thermoplastic materials, such as PPS, PEEK and PEKK etc., as their surface activities are typically very poor [28]. However, there is still a lack of research on this topic.

Herein, intermediate non-woven mats consisting of rCF and PPS fibres were compression moulded to manufacture rCF/PPS composites. The rCFs within the non-woven mats served as the reinforcement of the rCF composite, while the PPS fibres within the non-woven mats melted during the compression moulding and became the matrix of the rCF composites. The commingling of rCFs and PPS fibres within the non-woven mats allowed us to simultaneously treat the surfaces of the bi-fibres using a UV-treatment method, that proved to enhance the PPS/rCF interface strength within the rCF/PPS composites. The effects of the enhanced fibre/matrix interface on the interlaminar and intralaminar fracture resistance and mechanical performance of the rCF/PPS composites were investigated. The fracture surfaces and crack propagation path were also carefully analysed to explore the fracture mechanisms of the rCF/PPS composites.

2. Experimental

2.1. Material information and specimen manufacturing

The non-woven mats with an areal density of 100 g/m^2 were Carbiso-TM-PPS/60-IM56L-100, which were bought from ELG Carbon Fibre Ltd. The mats consisted of a blend of PPS and rCF bi-fibres, with the weight percentage of the rCFs being 40%. The rCFs were produced using a pyrolysis method by the supplier from the carbon fibre prepreg waste of Airbus, and they possessed an intermediate modulus of 5–6 GPa. Typical photographs and micrographs of the non-woven rCF/PPS mats are presented in Fig. 1. The average diameter of the rCFs and PPS fibres was 5.8 ± 0.3 μm and 15.7 ± 0.5 μm, respectively.

Prior to the compression moulding, the non-woven mats were firstly placed in an enclosed chamber, which has five 30 W UVC-lamps located at the ceiling of the chamber. The distance between the UV-lamps and the non-woven mats was approximately 50 mm. Both sides of the rCF/PPS non-woven mats were UV-treated. To analyse the influences of the surface treatment on the mechanical properties of the PPS fibres, a RSA-G2 Solid Analyser (from TA Instruments) was used to measure the mechanical properties of the single PPS fibre prior to and after different durations of UV-treatment. It should be noted that the PPS fibres for the single fibre tensile tests were the same grade material as the ones in the non-woven mats, that possessed an average diameter of 34 μm. After the surface treatment, the non-woven mats were laid together to prepare a dry layup, which were then compression-moulded in a hot-press by following the schedule that is schematically shown in Fig. 2. The consolidation schedule was suggested by the supplier, which can be divided into layup loading (I), press close with full pressure applied and heating up (II), consolidation (III) and pressure off and cooling down (IV) stages. The consolidation stage had the most significant influence on the composite quality, which was set as at 40 bar and 320 °C for 30 min. Composites based on 56 layers of non-woven mats and 32 layers of non-woven mats were manufactured to meet the requirements of different ASTM testing standards, that resulted in a thickness of about 4.0 mm and 2.5 mm of the plates, respectively. The rCF/PPS plates were then cut into desired dimensions for the following tests using a diamond abrasive machine.

2.2. Test methods

A CT (compact-tension) test was used to measure the intralaminar fracture toughness of the rCF/PPS composites [29], with the test configuration being shown in Fig. 3(a). A drill coated with diamond film (from LMT Onsrud, USA) was used to machine the 8 mm loading holes of the CT specimens, during which, the specimen was held between two pieces of wood to avoid obvious fraying and delamination. A razor saw with a thickness of 0.8 mm was firstly used to cut out the notch and then a new Stanley razor blade was sawing across the notch root to sharpen the crack tip. The insert image of Fig. 3(a) shows the micrograph of the crack tip. The CT test was carried out with a testing speed of 0.2 mm/min, during which a high-speed camera was used to record the crack propagation. The intralaminar fracture energy (G_{IC}^{intra}) of the rCF/PPS composites was calculated using the following equation [29]:

$$G_{IC}^{intra} = \frac{K_{IC}^2}{\sqrt{2E^2}}\sqrt{1+\frac{E}{2G}-\nu} \tag{1}$$

where K_{IC} is the critical stress intensity factor, E, G and ν are the in-plane Young's modulus, shear modulus and Poison's ratio of the rCF/PPS composites, respectively. K_{IC} is given as:

$$K_{IC} = \frac{P}{h\sqrt{w}} f(a/w) \tag{2}$$

with

$$f(a/w) = \frac{2+a/w}{(1-a/2)^{1.5}}[-5.6(a/w)^4 + 14.72(a/w)^3 - 13.32(a/w)^2 + 4.64(a/w) + 0.886] \tag{3}$$

where P is the load, w is the distance between the loading-line and the left edge of the specimen in Fig. 3(a), h is the specimen thickness and

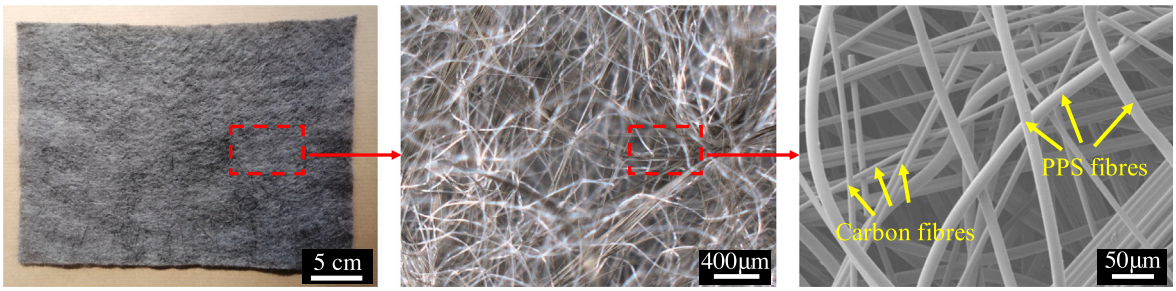

Fig. 1. Photographs and micrographs of the non-woven rCF/PPS mats.

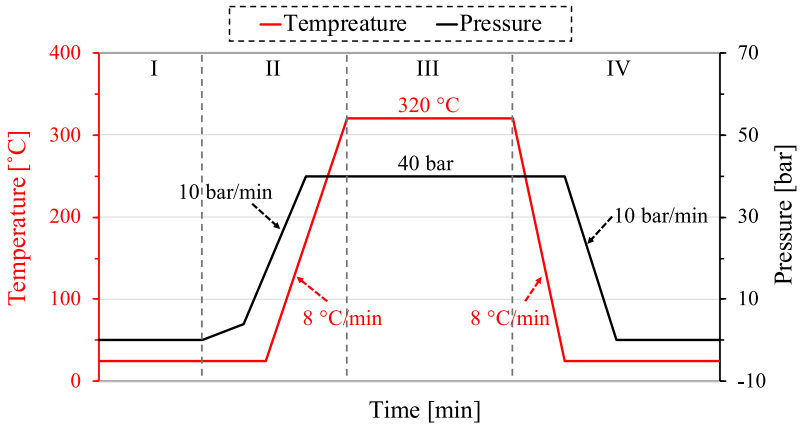

Fig. 2. Consolidation schedule of the composites based on rCF/PPS non-woven mats.

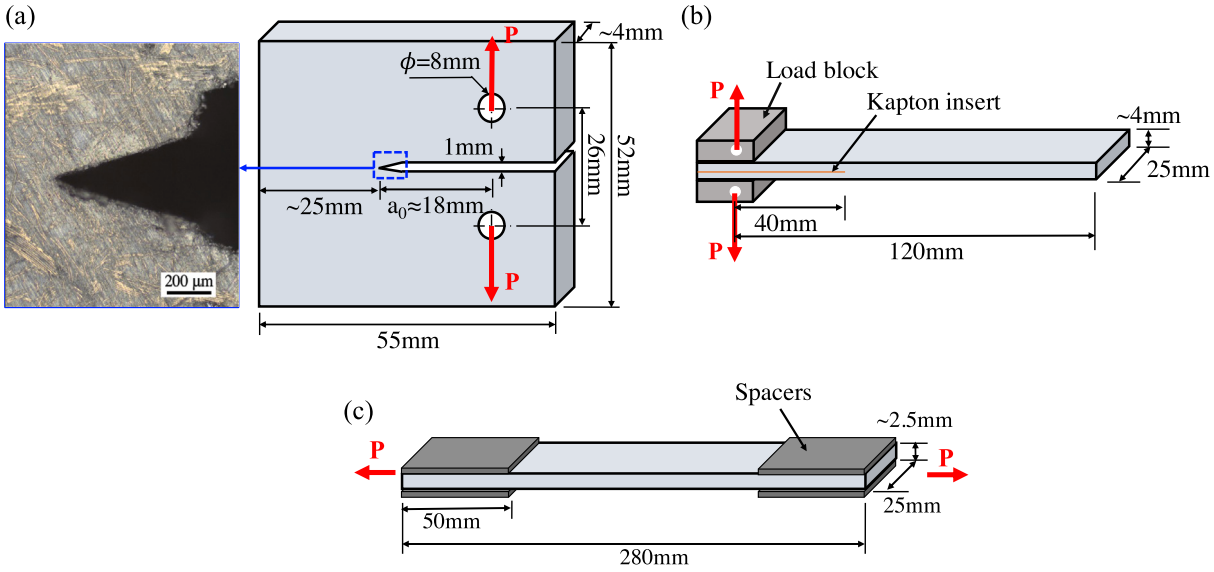

Fig. 3. The configurations of the: (a) compact-tension (CT) test, (b) double cantilever beam (DCB) test and (c) universal tensile test.

a is the distance between the crack tip and the loading line. Five tests were repeated in each case.

The interlaminar fracture behaviour of the rCF/PPS composite was evaluated using a DCB (double-cantilever beam) test [30], which is shown in Fig. 3(b). The crack starter of the DCB specimens was generated by inserting a layer of thin Kapton film into the laminate layup prior to the curing. The two surfaces of the Kapton film were coated with a release agent (Marbocote 227-CEE) to avoid any adhesion with the composite matrix. The DCB test was carried out at 3 mm/min, that was repeated for five times in each case. The interlaminar fracture energy (G_{IC}^{inter}) was derived using a modified beam theory [30]:

$$G_{IC}^{inter} = \frac{3P\delta}{2b(a+|\Delta|)} \tag{4}$$

where P, a and b are the load, length of the crack and specimen width, respectively, while δ is the displacement at the loading point. Δ was the correction factor for the beam rotation [30].

The tensile mechanical properties of the rCF/PPS composites were characterised according to ASTM-D3039 [31]. The testing configuration is shown in Fig. 3(c) The tests were carried out at a testing speed of 1 mm/min. Each test were repeated for five times.

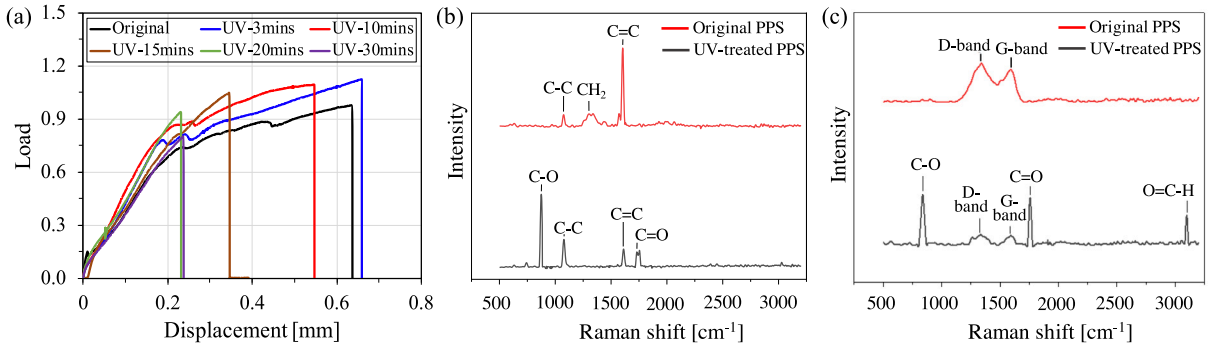

Fig. 4. (a) load–displacement curves of the single fibre tests of the PPS fibres. (b) and (c) the Raman spectrum curves of the non-treated and UV-treated rCFs and PPS fibres [32].

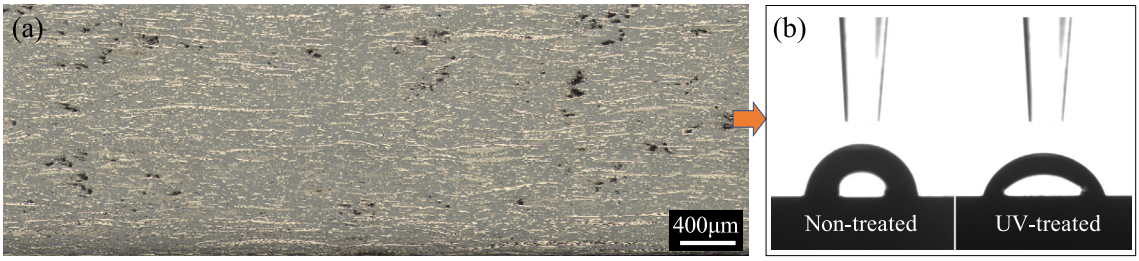

Fig. 5. (a) Micrograph of the cross-section of the rCF/PPS composites and (b) the corresponding water contact angle measurements.

The cross-section of the rCF/PPS composite was analysed using a laser microscope (KEYENCE VK-X1000), with the specimen being firstly grounded and polished. The void content of the composite was then calculated from the micrographs of the cross-section using an ImageJ software. The water contact angle of the polished cross-section was also investigated using a contact angle meter (from Attension Theta). SEM analysis was carried out to the interlaminar and intralaminar fracture surfaces of the composites using a scanning electron microscope (JSM-7500F from JOEL). The in-plane morphology of the CT specimens was imaged using the laser microscope to analyse the crack propagation path.

3. Results and discussion

3.1. Physical characterisation of the non-woven mat and rCF/PPS composite

Fig. 4(a) shows typical load–displacement curves from the single fibre tensile tests of the PPS fibres. Obviously, applying the UV-treatment for less than 10 min had no obvious effect on the mechanical properties of the PPS fibres. However, the plasticity or ductility of the PPS fibres considerably dropped while the treatment time was 15 min and above. According to the tensile test results in Fig. 4(a), a period of 10 min was selected for the UV-treatment that was applied to the rCF/PPS mats in this study. This treatment schedule assured that the surfaces of the bi-fibres were sufficiently activated, and moreover, no negative effect to the mechanical properties of the PPS fibres was induced by the UV-treatment.

Fig. 4(b) and (c) present the spectrum curves that were obtain from a Raman analysis on the rCFs and PPS fibres before and after the UV-treatment [32]. It was obvious that the quantity of oxygen-functional groups on the rCF and PPS surfaces dramatically increased upon the UV-treatment. This could prompt the level of chemical bonds at the rCF/PPS matrix interface, and subsequently improved the interface strength [23,33]. An improved interface adhesion had obvious influences on the fracture resistance and mechanical performance of the rCFRPs, which will be shown later on.

A typical micrograph of the cross-section of the rCF/PPS composites is shown in Fig. 5(a), and the results of the water contact angle measurements are shown in Fig. 5(b). It should be noted that no difference in the cross-section morphology was observed between the non-treated and UV-treated rCF/PPS composites. Many void defects in a black colour were observed in the rCF/PPS composites, which is typical for the rCFRPs. The area ratio of the voids was measured to be 3.55%, which was almost half of the value obtained in the reference [11]. The lower void content obtained in this study was because of the rCF/PPS composites were manufactured from co-mingled rCF/PPS fibre mats, which required less diffusion and flow of the PPS melt during the composite consolidation. However, the resin matrix layers and the pure rCF mats were individually laid together in [11], and hence the matrix had to flow into the rCF mats and impregnated them. From Fig. 5(b), it was observed that the water contact angle of the rCF/PPS composites decreased from 82.8 ± 2.3° to 72.2 ± 1.2° upon the UV-treatment. This corresponded well to the previous observation that the surfaces of the UV-treated PPS and rCFs possessed a larger number of polar oxygen groups, see Fig. 4(b) and (c). Additionally, the improved surface wetability of the rCF/PPS composites could be appealing for adhesive bonding or co-cure joining of the composites if these are required for the component assembly [28,34].

3.2. Intralaminar fracture of the rCF/PPS composite

The *R*-curves and intralaminar fracture energies (G_{IC}^{intra}) of the non-treated and UV-treated rCF/PPS composites are shown in Fig. 6. Fig. 6(a) shows that the values of the intralaminar fracture energies significantly changed with the crack length for all the CT specimens. This was because of the orientation and distribution of the rCFs were locally non-uniform along the crack-propagation path. Overall, the *R*-curves of the UV-treated rCF/PPS composite were above the ones for their non-treated counterparts, which resulted in higher G_{IC}^{intra} of the UV-treated composites in Fig. 6(b). In specific, the average value of G_{IC}^{intra} was measured to be 11.4 ± 0.7 kJ/m^2 for the non-treated rCF/PPS composites. Applying the surface treatment to the non-woven mats increases this value to 14.3 ± 0.5 kJ/m^2 for the UV-treated composites, corresponding to an increase of 25.7%.

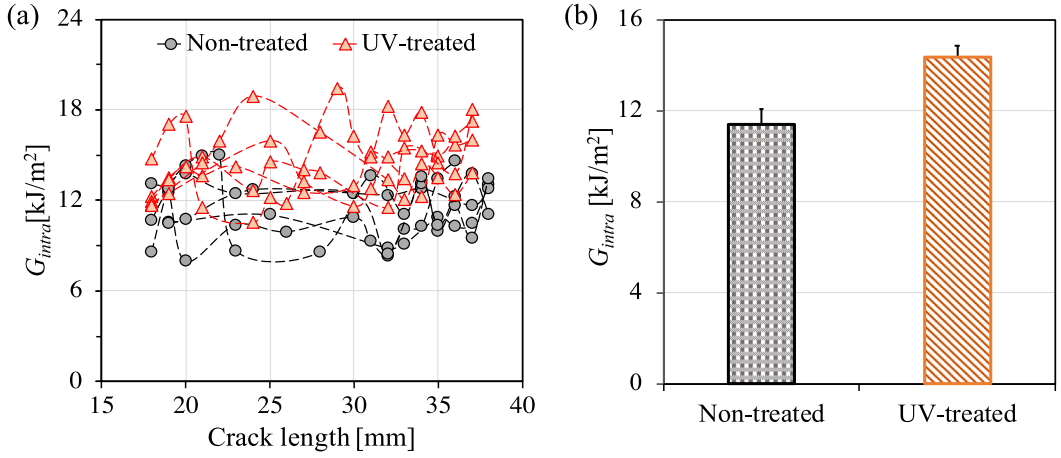

Fig. 6. Results of the intralaminar fracture tests: (a) the *R*-curves and (b) the intralaminar fracture energies.

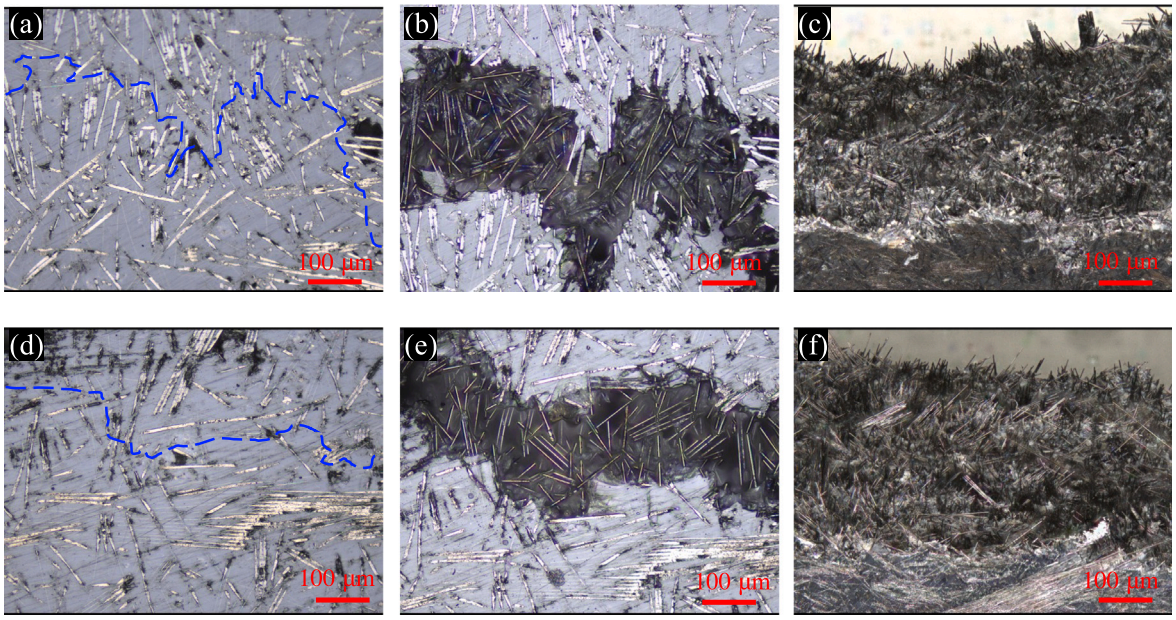

Fig. 7. Side-view of the CT specimens prior to the tests and after the tests. (a)–(c) are for the non-treated rCF/PPS composites and (d)–(f) are for the UV-treated composites. The blue dashed lines in (a) and (d) indicate the location of the fracture propagation routine prior to the fracture tests.

Fig. 7 shows the micrographs of the non-tested and tested intralaminar fracture specimens. The blue dashed lines in Fig. 7(a) and (d) indicate the crack routines of the specimens in the following tests. Overall, no obvious difference in the fracture phenomenon between the non-treated rCF/PPS composites and the UV-treated ones was observed. As shown in Fig. 7(b) and (e), a lot of rCFs had been pulled-out of the PPS matrix as the crack growing forward, which was the main fracture mechanism of the rCF/PPS composites in both cases. This fracture phenomenon corresponded well to the presence of numerous rCF segments on the intralaminar fracture surfaces in Fig. 7(c) and (f).

Fig. 8 shows typical SEM images on the intralaminar fracture surfaces of the rCF/PPS composites. By carrying out a careful comparison between Fig. 8(a) and (b), one can found that the surfaces of the pulled-out rCFs were relatively smooth for the non-treated composites, while the pulled-out rCFs were coated with a layer of plastic deformed and failed PPS resins for the UV-treated composite. This phenomenon had demonstrated an improved bonding strength at the rCF/PPS interface upon the UV-treatment. The increased interface strength resulted in higher pulling-out forces for the rCFs and more significant fracture of the PPS matrix, which contributed to the increased G_{IC}^{intra} by the UV-treatment, as shown in Fig. 6(b).

3.3. Interlaminar fracture properties of the rCF/PPS composite

Fig. 9 presents the *R*-curves, interlaminar fracture initiation energies (G_{inter}^{ini}) and fracture propagation energies (G_{inter}^{prop}) of the rCF/PPS composites. An obvious downturn in the *R*-curves were observed due to UV-irradiating the rCF/PPS mats, as can be seen in Fig. 9(a). Accordingly, the value of G_{inter}^{prop} decreased from 2.3 ± 0.3 kJ/m^2 of the non-treated composite to 1.9 ± 0.2 kJ/m^2 (by 17.4%) of the UV-treated composite, see Fig. 9(b). No obvious effect in G_{inter}^{ini} was observed upon the UV-treatment. For this reason, the difference between the values of G_{inter}^{prop} and G_{inter}^{ini} ($\Delta G_{inter} = G_{inter}^{prop} - G_{inter}^{ini}$) was much larger for the non-treated composites than the UV-treated composites. This was because of the increased rCF/PPS interface strengths by the UV-treatment affected the amount and effectiveness of the fibre bridging mechanism [35], as will be explained later on.

Fig. 10 presents photographs of the DCB specimens during the fracture tests. Significant bridging fibres were observed within the wake of the crack tips in both cases, as shown by Fig. 10(a) and (d). This indicates that rCF bridging was one of the main fracture mechanisms that contributed to the energy consumption. However, by carefully observing Fig. 10(b) and (e), it was observed that the length of the

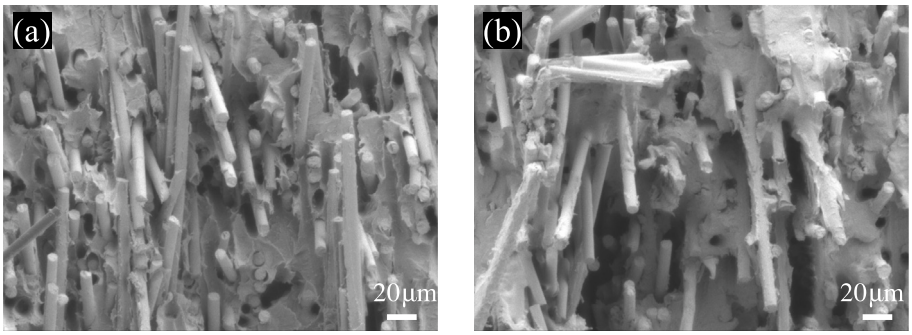

Fig. 8. Typical SEM images of the intralaminar fracture surfaces of the: (a) non-treated composites and (b) UV-treated composites.

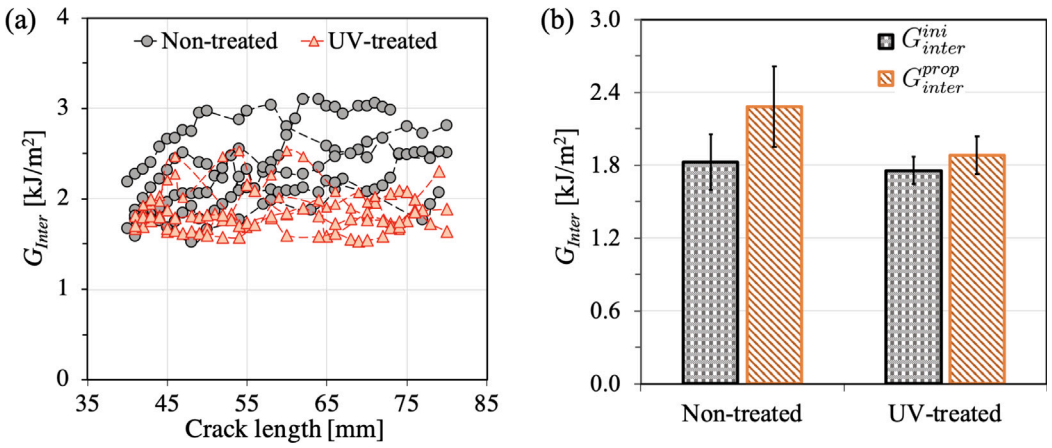

Fig. 9. Results of the interlaminar fracture tests: (a) the *R* curves and (b) the fracture energies.

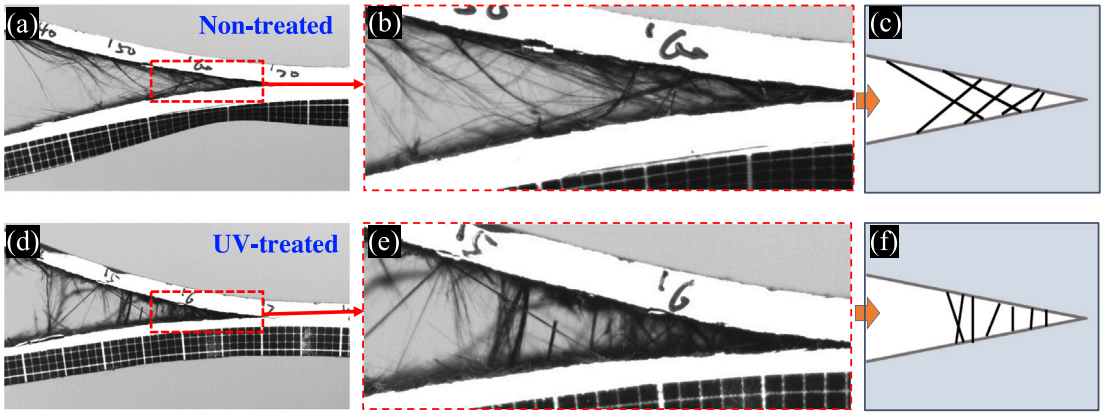

Fig. 10. Side-view images and schematics of the DCB specimens during the interlaminar fracture test of the: (a)–(c) non-treated composites and (d)–(f) UV-treated composites.

fibre bridging region was slightly longer for the non-treated rCF/PPS composites. More importantly, the bridging rCFs orientated more parallel to the crack growth direction for the non-treated composites and more perpendicularly to the crack growth direction for the UV-treated composites, as schematically shown by Fig. 10(c) and (f).

Fig. 11 presents SEM micrographs of the interlaminar fracture surfaces of the DCB specimens. From Fig. 11(a) and (b), it was observed that the fracture surfaces were characterised with a large number of delaminated rCFs in both cases, that corresponded well to the fibre bridging phenomenon observed in Fig. 10. However, the delaminated fibres individually distributed on the fracture surface of the non-treated composite, but in a cluster form for the UV-treated composites. Additionally, very smooth surfaces were observed for the delaminated rCFs and corresponding fibre prints on the fracture surfaces of the non-treated composite, see Fig. 10(c). This indicated relatively weak bonding strength at the PPS/rCFs interface. In contrast, the surfaces of the debonded carbon fibres for the UV-treated composites were covered with extensively damaged PPS matrix, as can be seen in Fig. 10(b) and (d). This was due to the enhanced PPS/rCF adhesion by the UV-treatment.

Based on these observations in Figs. 10 and 11, the interlaminar fracture mode of the rCF/PPS composites can be schematically shown as Fig. 12. While the crack front encountered a bundle of rCFs during the crack propagation process (Fig. 12(a)), the rCFs were prone to debond from the matrix for the non-treated composites owing to the relatively week PPS/rCF interface (Fig. 12(b)). In this case, continuous debonding and bridging of the rCFs took place without the edges of them being completely pulled-out. This resulted in a relatively longer

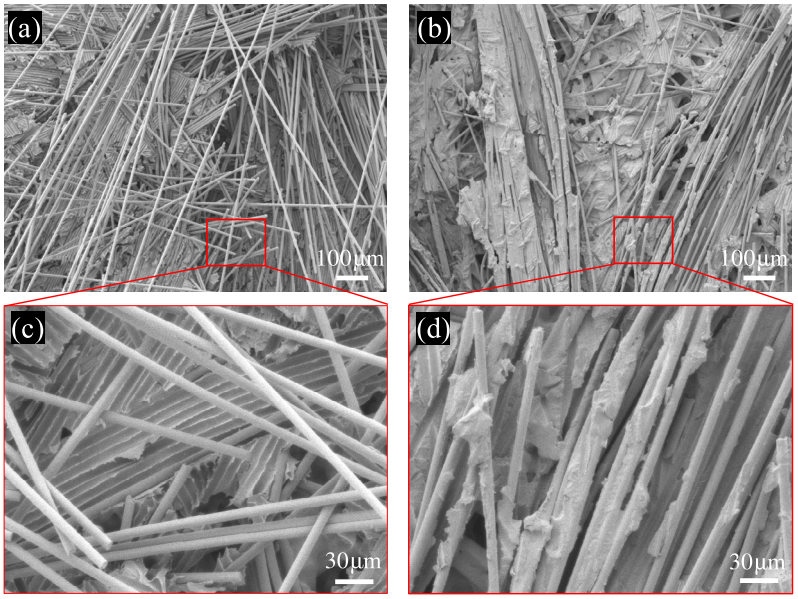

Fig. 11. Micrographs of the interlaminar fracture surfaces of the composites. (a) and (c) are for the non-treated composites, (b) and (d) are for the UV-treated composites.

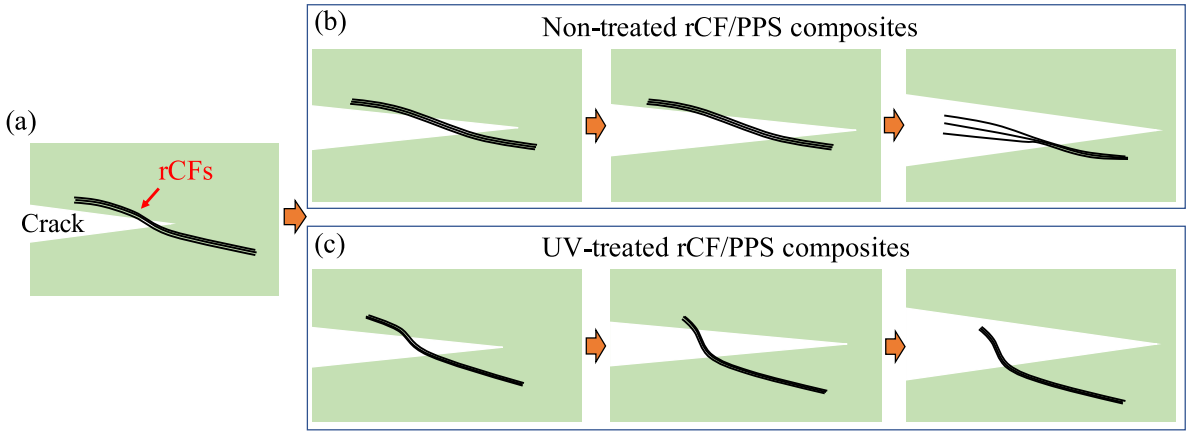

Fig. 12. Schematics for showing the fibre bridging phenomenon during the interlaminar fracture tests.

fibre bridging region, a larger number of rCFs for crack bridging and a more parallel orientation of the bridging fibres, as had been observed in Fig. 10(c). In the case of the UV-treated composites, the enhanced PPS/rCF interface led to a larger debonding force of the rCFs during the crack propagation process. This resulted in the more perpendicular orientation of the bridging rCFs in Fig. 10(f), and the relatively easier evulsion of one edge of the rCF bundle, as shown in Fig. 12(c). Overall, while the improved interface adhesion induced additional plastic deformation and damage to the PPS matrix, it also considerably reduced the amount and effectiveness of the main fibre bridging mechanism. This explained why G_{inter}^{prop} decreased upon the UV-treatment, as shown in Fig. 9(b).

3.4. Mechanical performance of the rCF/PPS composites

The tensile test results of the rCF/PPS composites are presented in Fig. 13. From Fig. 13(a), it was observed that the load–displacement curves were not strictly linear at the early stage for both of the non-treated and UV-treated CF/PPS composites. This was attributed to the stochastic distribution of the rCFs within the composites, i.e. some of the rCFs were loaded earlier, leading to gradual fibre pull-out phenomena. An improved PPS/rCF bonding strength upon the UV-treatment effectively increased the mechanical properties of the corresponding composites. In particular, the tensile modulus (E) and tensile strength had been increased from 17.5 GPa and 200.3 MPa to 20.4 GPa and 228.3 MPa, respectively. That corresponded to an increase of 16.5% and 14%, respectively, as can be seen from Fig. 13(b) and (c). The improvement in the mechanical properties was because of the enhanced PPS/rCF bonding strength promoted the load transfer between the rCFs and the PPS matrix, which utilised the good mechanical properties of the rCFs more effectively for load bearing.

4. Conclusions

This study applied a UV-treatment method to treat the non-woven mats consisting of recycled carbon fibres (rCFs) and PPS fibres, that proved to enhance the surface activities of the PPS and rCFs. Consequently, the interface strength between the PPS matrix and the rCFs had been promoted for the rCF/PPS composites that were compression moulded based on the rCF/PPS non-woven mats. The improvement of the PPS/rCF interface strength yielded significant improvements in the intralaminar fracture resistance and tensile and shear mechanical performance of the composites, but also caused considerable drop in the interlaminar fracture energy. The different influences in the intralaminar and interlaminar fracture properties were due to the different fracture mechanisms. The pulling-out of rCFs from the PPS matrix was

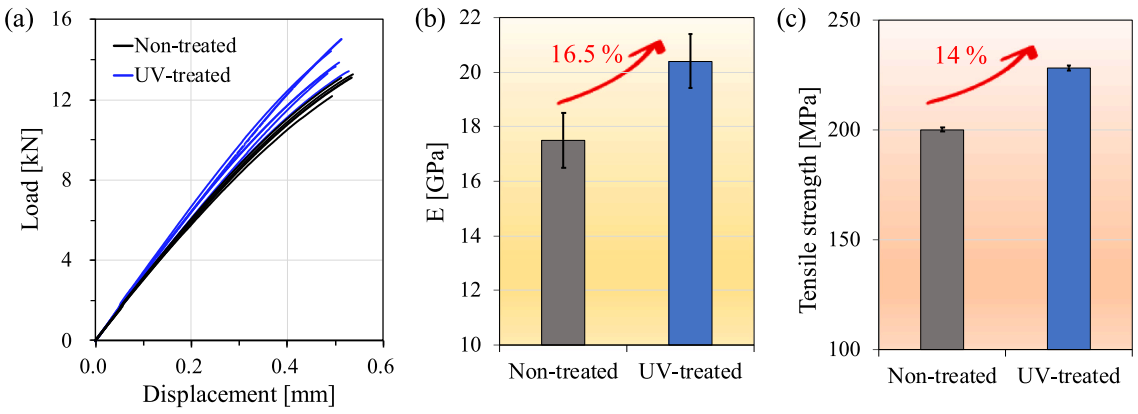

Fig. 13. The results of the tensile test: (a) load–displacement curves, (b) the Young's modulus and (c) the tensile strength.

determined to be the main fracture mechanism of the intralaminar fracture process, in which case, an improved adhesion increased the pulling-out forces and promoted the energy consumption. However, the main fracture mechanism of the interlaminar fracture process was fibre bridging, whose effectiveness and level for energy dissipation were negatively affected by the improved adhesion. Overall, the feasibility of developing advanced rCFRPs by tailoring the rCF/matrix adhesion had been proved by the experimental results of this work.

CRediT authorship contribution statement

Dong Quan: Conceptualization, Investigation, Methodology, Writing – original draft. **Jiaming Liu:** Methodology, Investigation. **Liaojun Yao:** Conceptualization, Investigation. **Clemens Dransfeld:** Methodology, Investigation. **René Alderliesten:** Conceptualization, Resources. **Guoqun Zhao:** Project administration, Funding acquisition.

Declaration of competing interest

The authors declare that they have no known competing financial interests or personal relationships that could have appeared to influence the work reported in this paper.

Data availability

Data will be made available on request.

Acknowledgements

The author is grateful to the financial support from Natural Science Foundation of Shandong Province, China (Grant No. : 2022HWYQ-013) and the key research and development program of Shandong Province (Grant No. 2021ZLGX01). Liaojun Yao would acknowledge the financial support from the National Natural Science Foundation of China (11902098,12272110), the Aeronautical Science Foundation of China (Grant No. 20200009077001) and the Natural Science Foundation of Heilongjiang Province, China (Grant No. LH2020A005).

References

[1] P. Xu, J. Li, J. Ding, Chemical recycling of carbon fibre/epoxy composites in a mixed solution of peroxide hydrogen and N,N-dimethylformamide, Compos. Sci. Technol. 82 (2013) 54–59, http://dx.doi.org/10.1016/j.compscitech.2013.04.002.

[2] E. Pakdel, S. Kashi, R. Varley, X. Wang, Recent progress in recycling carbon fibre reinforced composites and dry carbon fibre wastes, Resour. Conserv. Recy. 166 (2021) 105340, http://dx.doi.org/10.1016/j.resconrec.2020.105340.

[3] C.-H. Chen, C.-L. Chiang, J.-X. Wang, M.-Y. Shen, A circular economy study on the characterization and thermal properties of thermoplastic composite created using regenerated carbon fiber recycled from waste thermoset CFRP bicycle part as reinforcement, Compos. Sci. Technol. 230 (2022) 109761, http://dx.doi.org/10.1016/j.compscitech.2022.109761.

[4] S. Naqvi, H.M. Prabhakara, E. Bramer, W. Dierkes, R. Akkerman, G. Brem, A critical review on recycling of end-of-life carbon fibre/glass fibre reinforced composites waste using pyrolysis towards a circular economy, Resour. Conserv. Recy. 136 (2018) 118–129, http://dx.doi.org/10.1016/j.resconrec.2018.04.013.

[5] K. Kawajiri, M. Kobayashi, Cradle-to-Gate life cycle assessment of recycling processes for carbon fibers: A case study of ex-ante life cycle assessment for commercially feasible pyrolysis and solvolysis approaches, J. Clean. Prod. 378 (2022) 134581, http://dx.doi.org/10.1016/j.jclepro.2022.134581.

[6] Z. shang Tian, Y. qi Wang, X. lin Hou, Review of chemical recycling and reuse of carbon fiber reinforced epoxy resin composites, New Carbon Mater. 37 (6) (2022) 1021–1041, http://dx.doi.org/10.1016/S1872-5805(22)60652-8.

[7] S. Pimenta, S.T. Pinho, Recycling carbon fibre reinforced polymers for structural applications: Technology review and market outlook, Waste Manage. 31 (2) (2011) 378–392, http://dx.doi.org/10.1016/j.wasman.2010.09.019.

[8] A. Yu, Y. Hong, E. Song, H. Kim, I. Choi, M. Goh, Advanced oxidative chemical recycling of carbon-fiber reinforced plastic using hydroxyl radicals and accelerated by radical initiators, J. Ind. Eng. Chem. 112 (2022) 193–200, http://dx.doi.org/10.1016/j.jiec.2022.05.011.

[9] J. Wolling, M. Schmieg, F. Manis, K. Drechsler, Nonwovens from recycled carbon fibres - Comparison of processing technologies, Procedia CIRP 66 (2017) 271–276, http://dx.doi.org/10.1016/j.procir.2017.03.281.

[10] P. Bajpai, Chapter 7 - Manufacturing of composites from recycled carbon fiber, in: P. Bajpai (Ed.), Carbon Fiber (Second Edition), second ed., Elsevier, 2021, pp. 125–138, http://dx.doi.org/10.1016/B978-0-12-821890-7.00007-0.

[11] S. Pimenta, S.T. Pinho, P. Robinson, K.H. Wong, S.J. Pickering, Mechanical analysis and toughening mechanisms of a multiphase recycled CFRP, Compos. Sci. Technol. 70 (12) (2010) 1713–1725, http://dx.doi.org/10.1016/j.compscitech.2010.06.017.

[12] H. Wei, W. Nagatsuka, H. Lee, I. Ohsawa, K. Sumimoto, Y. Wan, J. Takahashi, Mechanical properties of carbon fiber paper reinforced thermoplastics using mixed discontinuous recycled carbon fibers, Adv. Compos. Mater. 27 (1) (2018) 19–34, http://dx.doi.org/10.1080/09243046.2017.1334274.

[13] H. Yu, K. Potter, M. Wisnom, A novel manufacturing method for aligned discontinuous fibre composites (High Performance-Discontinuous Fibre method), Composites A 65 (2014) 175–185, http://dx.doi.org/10.1016/j.compositesa.2014.06.005.

[14] H. Yu, M.L. Longana, M. Jalalvand, M.R. Wisnom, K.D. Potter, Pseudo-ductility in intermingled carbon/glass hybrid composites with highly aligned discontinuous fibres, Composites A 73 (2015) 35–44, http://dx.doi.org/10.1016/j.compositesa.2015.02.014.

[15] M.L. Longana, N. Ong, H. Yu, K.D. Potter, Multiple closed loop recycling of carbon fibre composites with the HiPerDiF (High Performance Discontinuous Fibre) method, Compos. Struct. 153 (2016) 271–277, http://dx.doi.org/10.1016/j.compstruct.2016.06.018.

[16] K. Wong, S. Pickering, C. Rudd, Recycled carbon fibre reinforced polymer composite for electromagnetic interference shielding, Composites A 41 (6) (2010) 693–702, http://dx.doi.org/10.1016/j.compositesa.2010.01.012.

[17] G. Jiang, S.J. Pickering, Structure-property relationship of recycled carbon fibres revealed by pyrolysis recycling process, J. Mater. Sci. 51 (4) (2016) 1949–1958, http://dx.doi.org/10.1007/s10853-015-9502-2.

[18] M. Andideh, M. Esfandeh, Statistical optimization of treatment conditions for the electrochemical oxidation of PAN-based carbon fiber by response surface methodology: Application to carbon fiber/epoxy composite, Compos. Sci. Technol. 134 (2016) 132–143, http://dx.doi.org/10.1016/j.compscitech.2016.08.008.

[19] S. Wang, S. Zhang, Y. Yang, Z. Dong, G. Wang, Direct electrochemical grafting of crystalline PAEK macromolecule on carbon fiber to enhance the interfacial properties of PEEK/CF composites, Compos. Sci. Technol. 220 (2022) 109262, http://dx.doi.org/10.1016/j.compscitech.2022.109262.

[20] H. Li, M. Liebscher, J. Yang, M. Davoodabadi, L. Li, Y. Du, B. Yang, S. Hempel, V. Mechtcherine, Electrochemical oxidation of recycled carbon fibers for an improved interaction toward alkali-activated composites, J. Clean. Prod. 368 (2022) 133093, http://dx.doi.org/10.1016/j.jclepro.2022.133093.

[21] B.-G. Cho, S.-H. Hwang, M. Park, J.K. Park, Y.-B. Park, H.G. Chae, The effects of plasma surface treatment on the mechanical properties of polycarbonate/carbon nanotube/carbon fiber composites, Composites B 160 (2019) 436–445, http://dx.doi.org/10.1016/j.compositesb.2018.12.062.

[22] M. Baghery Borooj, A. Mousavi Shoushtari, A. Haji, E. Nosratian Sabet, Optimization of plasma treatment variables for the improvement of carbon fibres/epoxy composite performance by response surface methodology, Compos. Sci. Technol. 128 (2016) 215–221, http://dx.doi.org/10.1016/j.compscitech.2016.03.020.

[23] H. Lee, I. Ohsawa, J. Takahashi, Effect of plasma surface treatment of recycled carbon fiber on carbon fiber-reinforced plastics (CFRP) interfacial properties, Appl. Surf. Sci. 328 (2015) 241–246, http://dx.doi.org/10.1016/j.apsusc.2014.12.012.

[24] D. He, V.K. Soo, F. Stojcevski, W. Lipiński, L.C. Henderson, P. Compston, M. Doolan, The effect of sizing and surface oxidation on the surface properties and tensile behaviour of recycled carbon fibre: An end-of-life perspective, Composites A 138 (2020) 106072, http://dx.doi.org/10.1016/j.compositesa.2020.106072.

[25] Y. Fu, H. Li, W. Cao, Enhancing the interfacial properties of high-modulus carbon fiber reinforced polymer matrix composites via electrochemical surface oxidation and grafting, Composites A 130 (2020) 105719, http://dx.doi.org/10.1016/j.compositesa.2019.105719.

[26] N. Feng, X. Wang, D. Wu, Surface modification of recycled carbon fiber and its reinforcement effect on nylon 6 composites: Mechanical properties, morphology and crystallization behaviors, Curr. Appl. Phys. 13 (9) (2013) 2038–2050, http://dx.doi.org/10.1016/j.cap.2013.09.009.

[27] G. Cai, M. Wada, I. Ohsawa, S. Kitaoka, J. Takahashi, Interfacial adhesion of recycled carbon fibers to polypropylene resin: Effect of superheated steam on the surface chemical state of carbon fiber, Composites A 120 (2019) 33–40, http://dx.doi.org/10.1016/j.compositesa.2019.02.020.

[28] D. Quan, R. Alderliesten, C. Dransfeld, I. Tsakoniatis, S. Teixeira De Freitas, G. Scarselli, N. Murphy, A. Ivanković, R. Benedictus, Significantly enhanced structural integrity of adhesively bonded PPS and PEEK composite joints by rapidly UV-irradiating the substrates, Compos. Sci. Technol. 199 (2020) 108358, http://dx.doi.org/10.1016/j.compscitech.2020.108358.

[29] ASTM Standard E399-20, Standard Test Method for Linear-Elastic Plane-Strain Fracture Toughness of Metallic Materials, ASTM International, 2020.

[30] ASTM Standard D5528-13(2013), Standard Test Method for Mode I Interlaminar Fracture Toughness of Unidirectional Fiber-Reinforced Polymer Matrix Composites, ASTM International, 2013.

[31] ASTM Standard D3039 (2017), Standard Test Method for Tensile Properties of Polymer Matrix Composite Materials, ASTM International, 2017.

[32] D. Quan, U. Farooq, G. Zhao, C. Dransfeld, R. Alderliesten, Recycled carbon fibre mats for interlayer toughening of carbon fibre/epoxy composites, Mater. Des. 218 (2022) 110671, http://dx.doi.org/10.1016/j.matdes.2022.110671.

[33] N. van de Werken, M.S. Reese, M.R. Taha, M. Tehrani, Investigating the effects of fiber surface treatment and alignment on mechanical properties of recycled carbon fiber composites, Composites A 119 (2019) 38–47, http://dx.doi.org/10.1016/j.compositesa.2019.01.012.

[34] D. Quan, R. Alderliesten, C. Dransfeld, I. Tsakoniatis, R. Benedictus, Co-cure joining of epoxy composites with rapidly UV-irradiated PEEK and PPS composites to achieve high structural integrity, Compos. Struct. 251 (2020) 112595, http://dx.doi.org/10.1016/j.compstruct.2020.112595.

[35] D. Quan, B. Deegan, R. Alderliesten, C. Dransfeld, N. Murphy, A. Ivanković, R. Benedictus, The influence of interlayer/epoxy adhesion on the mode-I and mode-II fracture response of carbon fibre/epoxy composites interleaved with thermoplastic veils, Mater. Des. 192 (2020) 108781, http://dx.doi.org/10.1016/j.matdes.2020.108781.